

PSA-MIL: A Probabilistic Spatial Attention-Based Multiple Instance Learning for Whole Slide Image Classification

Sharon Peled, Yosef E. Maruvka*, Moti Freiman*
Technion – Israel Institute of Technology, Haifa, Israel.
sharonpe@campus.technion.ac.il

Abstract

Whole Slide Images (WSIs) are high-resolution digital scans widely used in medical diagnostics. WSI classification is typically approached using Multiple Instance Learning (MIL), where the slide is partitioned into tiles treated as interconnected instances. While attention-based MIL methods aim to identify the most informative tiles, they often fail to fully exploit the spatial relationships among them, potentially overlooking intricate tissue structures crucial for accurate diagnosis. To address this limitation, we propose **Probabilistic Spatial Attention MIL (PSA-MIL)**, a novel attention-based MIL framework that integrates spatial context into the attention mechanism through learnable distance-decayed priors, formulated within a probabilistic interpretation of self-attention as a posterior distribution. This formulation enables a dynamic inference of spatial relationships during training, eliminating the need for predefined assumptions often imposed by previous approaches. Additionally, we suggest a spatial pruning strategy for the posterior, effectively reducing self-attention's quadratic complexity. To further enhance spatial modeling, we introduce a diversity loss that encourages variation among attention heads, ensuring each captures distinct spatial representations. Together, PSA-MIL enables a more data-driven and adaptive integration of spatial context, moving beyond predefined constraints. We achieve state-of-the-art performance across both contextual and non-contextual baselines, while significantly reducing computational costs. Our code is available at <https://github.com/SharonPeled/PSA-MIL>.

1. Introduction

Histopathological image analysis plays a crucial role in modern medicine, often regarded as ground truth in medical practice [15, 22, 22, 28]. The digitization of pathological slides into Whole Slide Images (WSIs) has revolution-

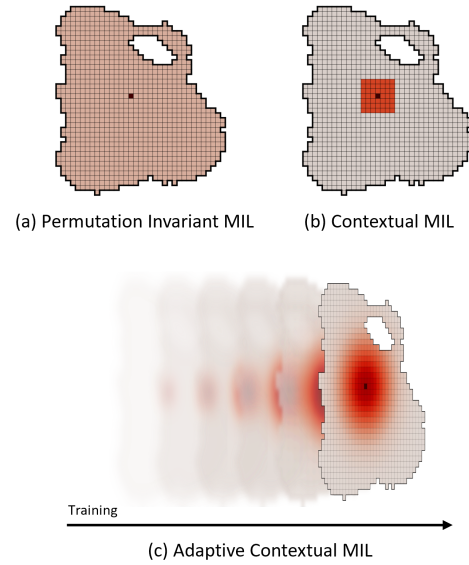


Figure 1. Conceptual Illustration of Implied Spatial Relationships from an Anchored Patch in Different MIL Paradigms.

(a) Permutation-invariant MIL treats all patches equally, disregarding spatial relationships. (b) Contextual MIL restricts interactions to a predefined neighborhood around the anchor patch, enforcing a fixed spatial structure. (c) Our proposed PSA-MIL dynamically learns spatial relationships, starting with an initial distribution over neighboring patches and evolving throughout training.

ized the field of pathology, enabling large-scale computational analysis. Due to the immense size of a WSI, which can exceed a billion pixels, a widely adopted approach for computational analysis is to decompose these large images into smaller, processable patches. Exhibiting only slide-level annotations, histopathological image analysis is commonly formulated as a Multiple Instance Learning (MIL) task [18, 42], where each slide is modeled as a permutation-invariant bag of instances, overlooking spatial dependencies among instances.

The incorporation of spatial context into MIL has gained popularity in recent WSI studies [9, 13, 25, 45]. While

*These authors are co-senior authors.

contextual models have shown strong performance, they often struggle to fully capture spatial dependencies among instances due to fixed spatial assumptions. For example, CAMIL [13] imposes predefined spatial constraints via a neighbor-constrained attention module, whereas Bayes-MIL [9] enforces spatial smoothness using a CRF with a fixed kernel size, both limiting flexibility in capturing diverse spatial patterns. Fig. 1 illustrates how different MIL paradigms model spatial relationships. Another popular approach for incorporating spatial context is positional encoding and its many variants [6, 25, 36, 45]. For example, SETMIL [45] employs Relative Positional Encoding (RPE) to model relative positions, HIPT [6] uses 2D absolute positional embeddings, and TransMIL [36] leverages PPEG, a convolution-based implicit positional encoding. While these methods have shown some performance gains, our experiments indicate that these improvements are often marginal. Moreover, their integration of spatial context is primarily empirically justified rather than theoretically grounded, resulting in a lack of a formal interpretative framework.

To this end, we propose **Probabilistic Spatial Attention MIL (PSA-MIL)**, a novel attention-based MIL approach that seamlessly integrates spatial context into the attention mechanism. Our method builds upon a probabilistic interpretation of self-attention, incorporating spatial relationships as learnable distance-decayed priors within a posterior distribution. This incorporation enables the model to capture how instances attend to each other based on their spatial proximity, balancing adaptive priors with observed likelihood. The main contributions of this paper can be summarized as follows:

- **A theoretically grounded formulation for spatial modeling:** We introduce a probabilistic self-attention framework that dynamically infers spatial dependencies during training rather than relying on predefined assumptions. This provides a principled and data-driven solution for leveraging spatial information in WSI analysis.
- **A spatial pruning strategy for computational efficiency:** We propose a spatial pruning strategy for the posterior distribution, significantly reducing the quadratic complexity of self-attention while preserving critical spatial dependencies. This results in substantial computational savings without compromising performance.
- **An entropy-based diversity loss for multi-head attention:** We introduce a loss term that explicitly encourages spatial variation among attention heads, ensuring that each head captures distinct spatial representations. This mitigates redundant representations often observed in multi-head architectures [2, 29, 43].

Together, these contributions make PSA-MIL a more data-oriented and adaptive framework for integrating spatial context, moving beyond predefined constraints and enabling a

principled approach to WSI analysis.

2. Related Work

2.1. Multiple Instance Learning in WSI Analysis

Multiple Instance Learning (MIL) has become a widely adopted approach for WSI classification, allowing models to make slide-level predictions using only weakly supervised, slide-level annotations [3, 4, 9, 42]. Given the high resolution and large scale of WSIs, MIL frameworks process slides as bags of image tiles (instances), enabling models to learn relevant diagnostic patterns without requiring exhaustive manual annotations. Attention-based Multi-Instance Learning (ABMIL) was introduced, allowing models to learn instance-level importance weights [18]. Several works have since refined feature aggregation. For example, CLAM [27] incorporated a prototype-based clustering mechanism, and DTFD-MIL [42] employed a multi-tier fusion strategy. More recently, Transformer-based MIL architectures have emerged, leveraging self-attention to capture long-range dependencies between tiles [4, 13, 36, 45]. For example, TransMIL [36] utilized pairwise token interactions, enabling the model to encode global and local features. GTP [46] combined Graph Neural Networks (GNNs) with Transformers, enabling topology-aware modeling of spatial relationships within WSIs.

2.2. Spatial Context in Multiple Instance Learning

Spatial understandings of tissue structures are crucial during histopathological examination [17, 23, 35]. Reflecting this clinical importance, several approaches have been proposed for modeling spatial context in MIL. Multi-scale approaches, including HIPT [6], DS-MIL [24], and SETMIL [45], learn hierarchical representations spanning different magnifications. However, their hierarchical nature increases complexity, and adjacent tiles may be assigned to different regions, disrupting spatial continuity. Graph-based approaches explicitly model spatial relationships by treating tiles as graph nodes with structured dependencies [3, 4, 46]. For example, SM-MIL [4] applies a smoothness operator, enforcing gradual transitions in attention scores to better capture local dependencies. Although effective, these methods prune to over-smoothing, limiting the model’s ability to capture fine-grained spatial distinctions [5, 33]. Positional encoding methods introduce spatial bias into tile representations to enhance spatial awareness [6, 25, 36, 45]. For example, TransMIL [36] employs PPEG, a convolution-based positional encoding, while SETMIL [45] utilizes Relative Positional Encoding (RPE) to model spatial relationships. While proven effective, our experiments show that their performance gains are often marginal. Bayes-MIL [9] takes a different approach by incorporating spatial context through a Convolutional CRF, however, it still relies on a fixed ker-

nel size, which restricts its ability to adapt. More recent approaches utilize spatially constrained Transformer-based MIL architectures, where interactions are restricted to fixed neighborhoods. For example, CAMIL [13] enforces predefined spatial constraints through a neighbor-constrained attention mechanism, while Li et al. [25] applies a fixed attention mask to model local interactions, both limiting flexibility in capturing diverse spatial patterns. Moreover, due to the quadratic complexity of self-attention, Transformer-based MIL architectures [13, 36] often rely on self-attention approximations, such as Nyströmformer [41], which can lead to suboptimal performance [10, 14]. In contrast, our PSA-MIL approach dynamically infers spatial relationships during training, adapting to the underlying tissue structure without rigid constraints. This paradigm shift is illustrated in Fig. 1. Additionally, our spatial pruning strategy eliminates the need for self-attention approximations, ensuring efficiency without compromising performance.

3. Methodology

3.1. Background

Preliminaries Given a WSI, tissue regions are cropped into tiles and encoded using a pretrained frozen encoder $E(\cdot)$, forming an instance embeddings matrix $X \in \mathbb{R}^{n \times d}$.

3.1.1. Self-Attention for Multiple Instance Learning

Under the MIL framework, self-attention is utilized to model interactions among instances within a bag, enabling each instance (or tile) to attend to all other instances. Given a bag of instance embeddings $X \in \mathbb{R}^{n \times d}$, the self-attention operation computes queries Q , keys K , and values V matrices through linear projections of the embeddings. The attention is defined as:

$$H = \text{softmax} \left(QK^\top / \sqrt{d_k} \right) V \quad (1)$$

where $H \in \mathbb{R}^{n \times d_v}$ represents the attention-weighted interactions among instances. Here, d_v and d_k denote the dimensionalities of the values and keys matrices, respectively.

Multi-head Attention Each output sequence H forms an attention head. In multi-head attention, multiple heads are concatenated and then linearly projected to compute the final output:

$$\text{Multi-Head}(\{Q, K, V\}_{i=1}^h) = \text{Concat}(H_1, \dots, H_h)W$$

where $W \in \mathbb{R}^{hd_v \times hd_v}$ is the projection matrix, and h denotes the number of heads.

The resulting attention outputs are aggregated via a pooling operator to compute the slide prediction.

While this formulation effectively captures intra-bag dependencies, it inherently treats the instances as unordered elements without considering their spatial relationships. This lack of spatial context may hinder the model’s ability to recognize more intricate structures.

3.1.2. Self-Attention for Multiple Instance Learning as Posterior Distribution

In the context of MIL, self-attention mechanism can be interpreted as computing posterior distributions of each tile’s query vector q_i over all key vectors k_j , effectively modeling the attention process as a Gaussian Mixture Model (GMM) [30, 31]. Consider the query vector $q_i \in \mathbb{R}^{d_k}$ for tile i and the key vectors $k_j \in \mathbb{R}^{d_k}$ for tiles $j = 1, \dots, N$. Let $t \in \{0, 1\}^N$ be a one-hot encoded vector indicating the selection of key k_j . The distribution of the query vector q_i is modeled as:

$$p(q_i) = \sum_{j=1}^N \pi_j p(q_i | t_j = 1) = \sum_{j=1}^N \pi_j \mathcal{N}(q_i | k_j, \sigma^2 I) \quad (2)$$

where $\pi_j = p(t_j = 1)$ is the prior probability, and $\mathcal{N}(q_i | k_j, \sigma^2 I)$ denotes a Gaussian distribution with mean k_j and covariance $\sigma^2 I$.

The posterior probability that q_i corresponds to k_j is given by:

$$\begin{aligned} p(t_j = 1 | q_i) &= \frac{\pi_j \mathcal{N}(q_i | k_j, \sigma^2 I)}{\sum_{j'=1}^N \pi_{j'} \mathcal{N}(q_i | k_{j'}, \sigma^2 I)} \\ &= \frac{\pi_j \exp[-(\|q_i\|^2 + \|k_j\|^2)/2\sigma^2] \exp(q_i^\top k_j / \sigma^2)}{\sum_{j'} \pi_{j'} \exp[-(\|q_i\|^2 + \|k_{j'}\|^2)/2\sigma^2] \exp(q_i^\top k_{j'} / \sigma^2)} \end{aligned} \quad (3)$$

The self-attention operation described in Eq. (1) implies the following assumptions:

Assumption 1. The queries and keys are ℓ_2 -normalized, i.e., $\|q_i\| = \|k_j\| = 1$ for all i and j .

Assumption 2. The prior probabilities are uniform, i.e., $\pi_j = \frac{1}{N}$ for all j .

Assumption 3. The variance σ^2 is constant and set to $\sqrt{d_k}$ for all components.

Under these assumptions, the posterior probability simplifies to:

$$p(t_j = 1 | q_i) = \frac{\exp(q_i^\top k_j / \sqrt{d_k})}{\sum_{j'=1}^N \exp(q_i^\top k_{j'} / \sqrt{d_k})} \quad (4)$$

Thus, the posterior distribution $p(t_j = 1 | q_i)$ corresponds exactly to the attention weights computed by the standard self-attention, as in Eq. (1).

3.2. PSA-MIL for WSI Classification

In the context of WSIs, instances represent contiguous regions of tissue, and their spatial arrangement provides valuable diagnostic cues [17, 23, 35]. However, the self-attention MIL, as formulated in Sec. 3.1.2, inherently disregards spatial relationships among instances, which may

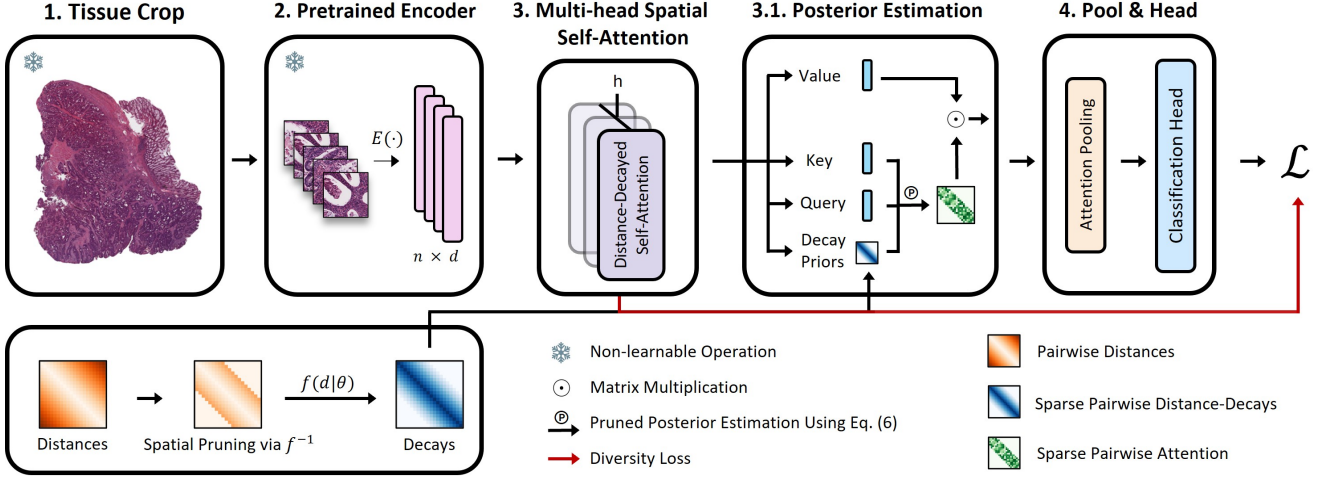


Figure 2. PSA-MIL Overview: 1-2. Tissue regions are cropped from the WSI, and the resulting tiles are encoded using a pretrained feature extractor, producing tile representations. 3-3.1. A Multi-Head Spatial Self-Attention mechanism is employed to generate informative, spatially correlated tile representations. Within this block, the pairwise distance matrix (bottom left) undergoes dynamic spatial pruning via the learned function $f^{-1}(\tau|\theta)$, producing a spatially pruned distance matrix. The distance-decayed matrix is then computed using $f(d|\theta)$. Both $f^{-1}(\tau|\theta)$ and $f(d|\theta)$ are learnable components parameterized by θ , enabling adaptive pruning and decay. Simultaneously, query, key, and value matrices are generated. The posterior attention distribution is then computed using Eq. (6) and applied to the value matrix, producing refined tile embeddings that encode spatial interactions. 4. These embeddings are subsequently pooled via an attention-based aggregation mechanism and passed through a classification head to generate slide-level predictions. The final loss function consists of both the classification loss and a diversity loss applied to the multi-head attention mechanism to encourage the capture of diverse spatial patterns.

limit the model’s ability to generalize. To this end, we propose PSA-MIL, a novel extension of the self-attention MIL that seamlessly integrates spatial context into the attention mechanism. Unlike previous approaches, our formulation enables an adaptive and principled spatial modeling without imposing predefined spatial constraints [9, 13, 25]. Building upon the probabilistic interpretation of self-attention described in Sec. 3.1.2, we relax both *Assumption 1* (ℓ_2 -normalized queries and keys) and *Assumption 2* (uniform priors), allowing for a more refined posterior estimation.

Relaxing Assumption 1 ℓ_2 -normalization of queries and keys is often introduced to align attention with a probabilistic interpretation [31]. However, standard self-attention does not inherently enforce this assumption, leading to inconsistencies in the formulation. We relax this assumption altogether and instead compute the full ℓ_2 -norm $\|q_i - k_j\|^2$, allowing queries and keys to retain magnitude information, which can enhance expressiveness [31].

Relaxing Assumption 2 We relaxed Assumption 2 by replacing the uniform priors with learnable, distance-decayed priors, enabling the capture of spatial relationships among instances. These priors are modeled as parametric, learnable functions, providing a structured and interpretable framework for spatial context.

Pooling Operator The [CLS] token is a common pooling strategy in transformers [12], effective for aggregating in-

formation across multiple self-attention layers. Our model employs a single-layer, multi-head self-attention architecture for an optimal balance between performance and efficiency. Consequently, we adopt attention-based pooling instead of the [CLS] token, leveraging its enhanced interpretability.

Fig. 2 depicts the complete PSA-MIL pipeline for spatial context modeling in WSI analysis.

3.2.1. Refined Posterior After Assumption Relaxation

Consider a set of instance embeddings $X \in \mathbb{R}^{n \times d}$, along with their corresponding pairwise distances $D \in \mathbb{R}^{n \times n}$, where d_{ij} represents the euclidean distance between tiles i and j . We define a learnable distance decay function $f(\cdot|\theta)$, where θ is learnable, and $f(d_{ij}|\theta)$ represents the decay for tile j from tile i .

Utilizing Eq. (3) for the posterior of q_i , we replace the uniform priors with spatially-informed priors assigned according to $f(\cdot|\theta)$:

$$\pi_j = p(t_j = 1) = f(d_{ij}|\theta) \quad (5)$$

and are learned during training.

For numerical stability, we incorporate these priors into the posterior distribution by embedding them directly within the exponentials. The overall posterior is then given by:

$$p(t_j = 1 | q_i) = \frac{\exp\left(\frac{\|q_i - k_j\|^2}{\sqrt{d_k}} + \log(f(d_{ij}|\theta))\right)}{\sum_{j'=1}^N \exp\left(\frac{\|q_i - k_{j'}\|^2}{\sqrt{d_k}} + \log(f(d_{ij'}|\theta))\right)} \quad (6)$$

This formulation enables the model to derive the spatial importance directly from the spatial correlations in the data, resulting in a more adaptive and context-aware representation. See full pipeline in Fig. 2.

Remark. $f(\cdot|\theta)$ can be interpreted as a form of regularization, constraining the model’s expressiveness by limiting information flow from distant instances.

3.2.2. Parametric Distance-Decay Functions for Spatial Modeling

As detailed in Eq. (5), the prior distribution is defined by the function $f(\cdot|\theta)$, which directly models the decay of influence over distance. Consequently, $f(\cdot|\theta)$ should satisfy the following properties:

1. Non-negativity: $f(d_{ij}|\theta) \geq 0$ for all j , $f(d_{ii}|\theta) > 0$.
 2. Monotonicity: $f(d_{ij}|\theta) \geq f(d_{ij'}|\theta)$ if $d_{ij} \leq d_{ij'}$.
- Note that the normalization factor $\sum_{j=1}^N f(d_{ij}|\theta)$ cancels out in Eq. (3).

However, learning $f(\cdot|\theta)$ directly is challenging due to the difficulty of enforcing these constraints during training. To address this, we adopt learnable parametric functions that provide a structured way for dynamically modeling spatial distance-decayed prior probabilities. We experiment with three parametric decay functions, each exhibiting distinct attenuation behavior:

1. Exponential Decay: $f(d|\lambda) = \exp(-\lambda d)$
Provides sharper attenuation, useful when influence drops off quickly with distance.
2. Gaussian Decay: $f(d|\sigma) = \exp\left(-\frac{d^2}{2\sigma^2}\right)$
Suitable for smoothly decreasing influence over distance, effective for modeling gradual spatial dependencies.
3. Cauchy Decay: $f(d|\gamma) = \frac{1}{1 + \left(\frac{d}{\gamma}\right)^2}$
Captures long-range dependencies, allowing distant tiles to retain influence due to its heavy-tailed nature.

These parametric decay functions provide a structured, learnable mechanism for adjusting spatial influence, enabling the model to adaptively capture varying spatial dependencies.

3.3. Spatially Pruning the Posterior

The quadratic computational complexity of self-attention presents a major challenge for long sequences, such as in WSI analysis. Proposed solutions include low-rank and kernel-based approximations [8, 20, 40, 41], such as

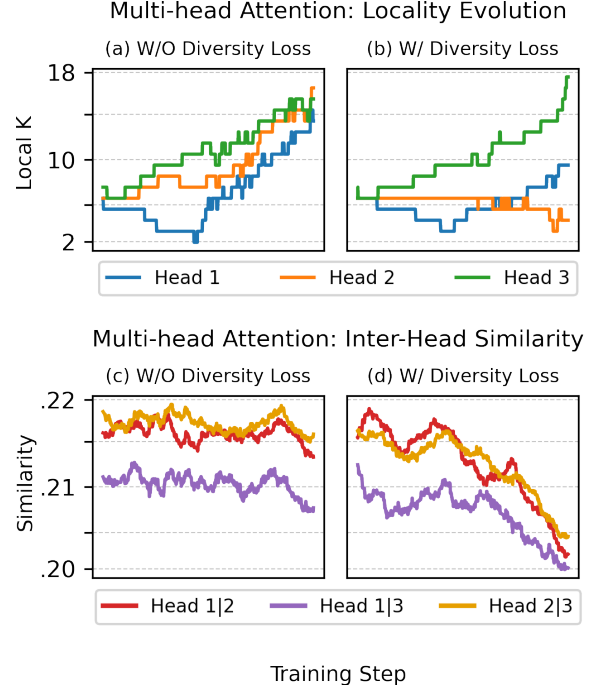


Figure 3. **The Effect of Diversity Loss on Multi-Head Attention.** (a-b). Locality evolution: Without diversity loss, all heads converge to similar locality values, whereas with diversity loss, the locality values diverge. (c-d). Inter-head similarity: The similarity metric measures average ℓ_2 token similarity (smoothed) across heads. Without diversity loss, similarity remains relatively high, while with diversity loss, similarity decreases, promoting diverse attention patterns. See Sec. 4.5 for additional details.

Nyströmformer [41] used in TransMIL [36] and in CAMIL [13]. Though, these approaches often yield sub-optimal performance [10, 14]. Other methods apply local attention, limiting focus to local context while stacking multiple layers to capture global interactions [25]. Although local self-attention reduces computation, it ultimately relies on fixed spatial assumptions, which limits its ability to fully model spatial dependencies.

To address this challenge, we propose a spatial pruning strategy for the posterior distribution, leveraging the inferred prior distribution during training to restrict attention computations based on learned spatial dependencies. Namely, we apply a filtering criterion $f(d|\theta) \geq \tau$, where τ is a threshold parameter, permitting only instances with decays above τ to contribute to the posterior computation. Such pruning techniques have been explored in mixture models, demonstrating the effectiveness of removing components that contribute negligibly to the posterior [32, 37]. Notably, by utilizing an invertible parametric function $f(d|\theta)$, we establish that $d \leq f^{-1}(\tau|\theta)$, effectively reducing our method to a form of K -local self-attention with $K = \lceil f^{-1}(\tau|\theta) \rceil$ and a computational complexity of

Method		TCGA-CRC			TCGA-STAD		
		AUC	Accuracy	F1 Score	AUC	Accuracy	F1 Score
Non-Contextual	ABMIL [18]	85.21 \pm 1.01	87.18 \pm 1.03	62.09 \pm 0.99	81.25 \pm 1.45	72.98 \pm 0.83	84.98 \pm 1.02
	CLAM [27]	86.18 \pm 0.96	87.72 \pm 1.61	64.81 \pm 1.35	81.71 \pm 0.72	76.32 \pm 0.89	85.35 \pm 0.72
	DTFD-MIL [42]	86.70 \pm 0.94	88.01 \pm 1.92	66.28 \pm 1.55	81.96 \pm 0.32	78.12 \pm 0.92	85.55 \pm 0.56
	IBMIL [26]	87.51 \pm 1.03	88.23 \pm 0.89	66.01 \pm 0.56	82.31 \pm 1.23	78.81 \pm 1.24	87.67 \pm 0.89
Contextual	TransMIL [36]	85.94 \pm 1.54	87.43 \pm 2.21	63.18 \pm 1.23	79.97 \pm 1.84	75.82 \pm 1.52	81.55 \pm 1.11
	GTP [46]	85.87 \pm 2.72	88.12 \pm 1.41	65.85 \pm 2.81	80.41 \pm 1.57	78.30 \pm 3.61	85.47 \pm 2.71
	SM-MIL [4]	87.84 \pm 0.45	88.86 \pm 0.29	64.60 \pm 2.53	81.23 \pm 1.37	79.79 \pm 1.88	87.85 \pm 0.57
	BAYES-MIL [9]	86.66 \pm 1.23	87.57 \pm 0.93	66.93 \pm 2.32	82.11 \pm 2.12	78.41 \pm 0.65	87.39 \pm 0.51
	PSA-MIL _[Exp]	88.27 \pm 0.94	88.13 \pm 0.92	66.29 \pm 1.55	82.96 \pm 0.92	78.48 \pm 0.87	89.28 \pm 1.01
	PSA-MIL _[Gau]	88.97 \pm 1.01	87.48 \pm 1.03	66.27 \pm 1.99	82.98 \pm 1.12	79.09 \pm 1.83	89.53 \pm 1.00
	PSA-MIL _[Cau]	87.50 \pm 1.04	88.93 \pm 1.21	67.70 \pm 1.23	83.06 \pm 0.57	78.59 \pm 0.45	89.52 \pm 1.31

Table 1. Performance comparison of different MIL approaches on TCGA-CRC and TCGA-STAD datasets, categorized into Non-Contextual and Contextual methods.

$O(n \cdot K^2) \ll O(n^2)$. Because $f(d|\theta)$ is learned during training, the locality of the self-attention is also learned, resulting in a *dynamic local attention*. Furthermore, unlike standard local self-attention, the retained instances are weighted by their learned decay values, making the operation spatially aware. Notably, we do not fine-tune τ ; instead, we typically set it to a constant value (e.g., $1e-3$), which we find works well in practice.

Fig. 2 illustrates how $f^{-1}(\tau|\theta)$ is applied in the PSA-MIL pipeline. Moreover, Fig. 3 (a-b) shows the evolution of our dynamic self-attention during training.

3.4. Diversity Loss for Spatial Decay Parameters

Multi-head attention allows the model to learn nuanced representations by having each head focus on different aspects of the input [38]. However, multi-head mechanisms are often prone to redundancy and entanglement, which can limit the diversity of learned representations and lead to suboptimal outcomes [2, 29, 43]. To overcome this issue, we suggest an entropy-based loss term that encourages diversity among $f(\cdot|\theta)$, enabling the model to capture diverse spatial patterns within the data.

Let θ_h be the spatial decay parameter for head h , drawn from an unknown distribution $p(\theta)$. To approximate $p(\theta)$, we use Kernel Density Estimation (KDE) [7]:

$$\hat{p}(\theta) = \frac{1}{H\sigma} \sum_{h=1}^H K\left(\frac{\theta - \theta_h}{\sigma}\right), \quad (7)$$

where $K(x)$ is a Gaussian kernel with bandwidth σ . To encourage variation among heads, we introduce an entropy-based loss term that promotes diversity in $\{\theta_h\}_{h=1}^H$. The entropy of $p(\theta)$ is given by: $H(p) =$

$-\mathbb{E}_{\theta \sim p(\theta)}[\log p(\theta)]$, which we estimate via Monte Carlo [16]:

$$H(p) \approx -\frac{1}{M} \sum_{m=1}^M \log \hat{p}(\tilde{\theta}_m), \quad (8)$$

where $\tilde{\theta}_m$ are samples drawn from $\hat{p}(\theta)$.

The entropy-based diversity loss is then defined as $\mathcal{L}_{\text{Diversity}} = -H(p)$ and incorporated into the final objective:

$$\mathcal{L} = \mathcal{L}_{\text{CE}} + \alpha \mathcal{L}_{\text{Diversity}}, \quad (9)$$

where \mathcal{L}_{CE} is the cross-entropy loss and α is a hyperparameter. By encouraging high entropy, PSA-MIL achieves a more disentangled and diverse spatial representations. Fig. 3 demonstrates the effect of the diversity loss on locality convergence and the disentanglement of representations.

4. Experiments

Datasets We validated our findings on two cancer subtyping tasks: Microsatellite Stable (MSS) vs. Microsatellite Instability (MSI) for colorectal adenocarcinoma (CRC) [1, 11] and Genomic Stability (GS) vs. Chromosomal Instability (CIN) for stomach adenocarcinoma (STAD) [39, 44]. Both datasets were sourced from The Cancer Genome Atlas¹ (TCGA) project. For details on clinical significance, slide counts, and label distribution, refer to Peled et al. [34]. In line with previous studies [13, 26, 36, 42], we assessed model performance primarily using the Area Under the Curve (AUC) metric, with Accuracy and F1 as secondary

¹<https://portal.gdc.cancer.gov>

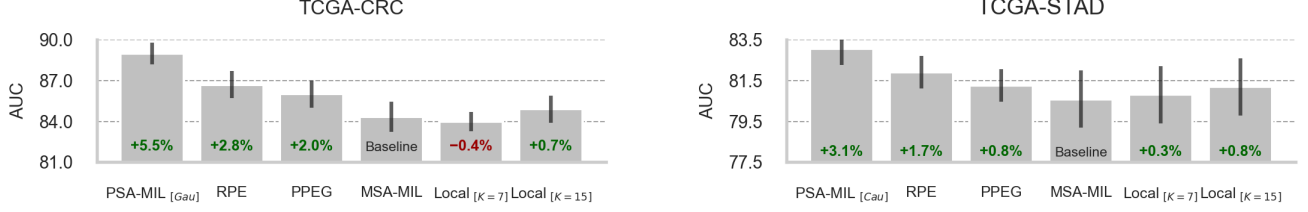


Figure 4. Performance comparison of different approaches for incorporating spatial context into self-attention MIL (MSA-MIL).

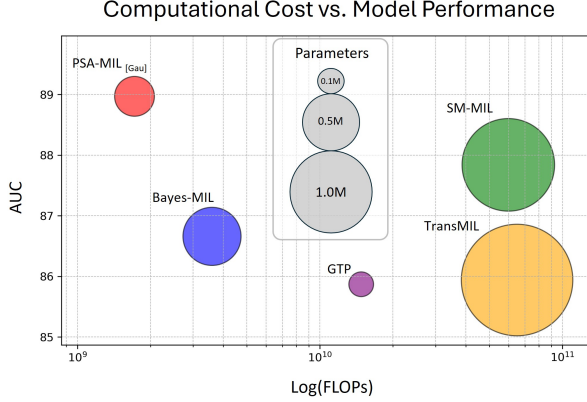


Figure 5. AUC on TCGA-CRC vs. FLOPs (log scale) for contextual MIL models, with bubble size representing parameter count.

measures. To ensure robustness, we obtained results using nested 5-fold cross-validation, repeated three times with different seeds.

Implementation Details All experiments used the foundation backbone from [19]. PSA-MIL architecture comprises a single layer with three 32-dim heads, $\tau = 10^{-3}$, and learning rate 10^{-4} . Experiments were conducted on an NVIDIA A100 GPU. Please refer to the supplementary for more details.

4.1. Benchmarking with Existing Works

We compare PSA-MIL to several contextual and non-contextual MIL baselines, concentrating on recent advancements in spatial modeling, such as SM-MIL [4], Bayes-MIL [9], and GTP [46]. The results are presented in Tab. 1.

Our PSA-MIL variants consistently outperform prior works across most metrics, demonstrating the effectiveness of learned spatial priors. Notably, non-contextual methods perform competitively compared to previous contextual approaches, with IBMIL even surpassing certain contextual models. This suggests that prior contextual methods may not fully capture spatial relationships effectively. Among contextual methods, SM-MIL demonstrates strong performance, highlighting the effectiveness of local smoothness in attention maps. Similarly, Bayes-MIL performs well,

particularly on TCGA-STAD, underscoring the advantages of probabilistic modeling. Furthermore, we observe performance differences among PSA-MIL variants, suggesting that spatial distribution modeling impacts performance.

4.2. Evaluating Spatial Context Integration in Self-Attention MIL

To further demonstrate the effectiveness of our approach, we compare it to several existing methods for integrating spatial context into self-attention MIL (MSA-MIL), described in Sec. 3.1.1. Specifically, we benchmark against three baselines: the naive approach (with no spatial context), K-local attention (where only instances within the K-neighborhood are included in the self-attention, each with equal contribution), PPEG used in TransMIL [36], and Relative Positional Encoding (RPE) suggest by SETMIL [45]. Fig. 4 presents the results. PSA-MIL achieved the best results on both datasets, outperforming the baseline by +5.5% in TCGA-CRC and +3.1% in TCGA-STAD. While positional encoding methods provided some improvement, their impact was significantly lower than ours, with RPE proving more effective than PPEG. The K-local attention variants yielded minimal to no performance gains, highlighting the limitations of fixed local constraints and the advantages of dynamic spatial modeling.

4.3. Computational Cost Analysis of Contextual MIL Models

Contextual MIL models inherently incur higher computational costs due to the need to model spatial interactions. To further demonstrate the superiority of our approach, we conduct a computational cost analysis, comparing AUC performance against FLOPs, with bubble sizes indicating the number of trained parameters. For this experiment, we utilized TCGA-CRC dataset. Fig. 5 presents the results.

PSA-MIL achieves the highest AUC while maintaining the lowest FLOP count and fewer parameters, indicating the effectiveness of our proposed spatial pruning strategy. SM-MIL showed good performance (Tab. 1) but requires significantly more computational resources. GTP has a small parameter footprint yet suffers from high FLOPs and inferior performance.



Figure 6. (A) Tumor segmentation using NCT-CRC-HE-100K [21]. (B-D) Attention heatmaps of individual heads in PSA-MIL_[Gau], illustrating diverse spatial focus. (E) Aggregated attention heatmap from the attention pooling operator.

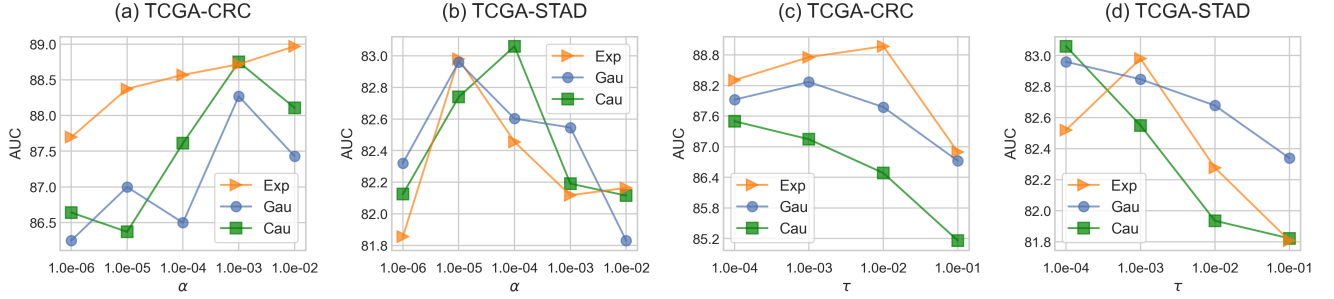


Figure 7. Ablation studies on the impact of α (a-b) and τ (c-d) in PSA-MIL.

4.4. Ablation Studies

4.4.1. Impact of α Value

Our approach employs diversity loss to encourage the capture of diverse spatial patterns. As shown in Fig. 7 (a-b), TCGA-CRC favored relatively higher α values, indicating the benefits of diverse representations. On the other hand, a moderate α value yields the best results across all decay functions for TCGA-STAD.

4.4.2. Impact of τ Value

Our approach leverages τ to regulate spatial pruning, controlling the range of spatial interactions in PSA-MIL. In our experiments, we typically set it to a constant value (e.g., $1e-3$), which we find works well in practice. As shown in Fig. 7 (c-d), Gaussian decay, which models gradual changes, remains relatively stable to variations in τ . In contrast, Cauchy decay, which favors long-range dependencies, is more sensitive, exhibiting steeper performance drops. Despite the expected performance drops, PSA-MIL maintains strong results even under significant computational constraints.

4.5. Training Dynamics and Attention Visualization

We analyze the training dynamics and attention patterns of PSA-MIL_[Gau] on the TCGA-CRC dataset, focusing on the impact of diversity loss and the learned spatial behaviors of attention heads.

Fig. 3 examines the evolution of the local-K in our dynamic local attention formulation. Without diversity loss (Fig. 3a), all heads converge to similar locality values, whereas with

diversity loss (Fig. 3b), they exhibit more distinct behaviors, ensuring diverse spatial representations. Similarly, inter-head similarity remains relatively high without diversity loss (Fig. 3c), while diversity loss (Fig. 3d) encourages head specialization by reducing pairwise similarity.

In Fig. 6, we visualize the attention heatmaps of PSA-MIL_[Gau]. All attention maps align with tumor regions, demonstrating the model’s ability to identify relevant areas. Additionally, we observe distinct attention behaviors across heads: head 2 ($K=4$) exhibits highly localized attention with dispersed activation spots, whereas head 3 ($K=17$) captures global dependencies with a smoother attention distribution. This reinforces the role of learned spatial priors in producing complementary attention patterns.

5. Conclusion

We introduce PSA-MIL, a novel approach for integrating spatial context into attention-based MIL through a probabilistic interpretation of self-attention as a posterior distribution. Unlike conventional MIL methods, which often fail to fully exploit spatial dependencies, PSA-MIL dynamically learns spatial relationships during training. Additionally, our entropy-based diversity loss promotes distinct spatial attention patterns across heads, further enhancing representation learning. Our experiments show that PSA-MIL outperforms existing methods while significantly reducing computational costs, highlighting its effectiveness in adaptive spatial modeling.

References

- [1] Martina Amato, Renato Franco, Gaetano Facchini, Raffaele Addeo, Fortunato Ciardiello, Massimiliano Berretta, Giulia Vita, Alessandro Sgambato, Sandro Pignata, Michele Caraglia, et al. Microsatellite instability: from the implementation of the detection to a prognostic and predictive role in cancers. *International journal of molecular sciences*, 23 (15):8726, 2022. 6
- [2] Yuchen Bian, Jiaji Huang, Xingyu Cai, Jiahong Yuan, and Kenneth Church. On attention redundancy: A comprehensive study. In *Proceedings of the 2021 conference of the north american chapter of the association for computational linguistics: human language technologies*, pages 930–945, 2021. 2, 6
- [3] Gianpaolo Bontempo, Federico Bolelli, Angelo Porrello, Simone Calderara, and Elisa Ficarra. A graph-based multi-scale approach with knowledge distillation for wsi classification. *IEEE Transactions on Medical Imaging*, 2023. 2
- [4] Francisco M Castro-Macías, Pablo Morales-Álvarez, Yunan Wu, Rafael Molina, and Aggelos K Katsaggelos. Sm: enhanced localization in multiple instance learning for medical imaging classification. *arXiv preprint arXiv:2410.03276*, 2024. 2, 6, 7
- [5] Deli Chen, Yankai Lin, Wei Li, Peng Li, Jie Zhou, and Xu Sun. Measuring and relieving the over-smoothing problem for graph neural networks from the topological view. In *Proceedings of the AAAI conference on artificial intelligence*, pages 3438–3445, 2020. 2
- [6] Richard J Chen, Chengkuan Chen, Yicong Li, Tiffany Y Chen, Andrew D Trister, Rahul G Krishnan, and Faisal Mahmood. Scaling vision transformers to gigapixel images via hierarchical self-supervised learning. In *Proceedings of the IEEE/CVF Conference on Computer Vision and Pattern Recognition*, pages 16144–16155, 2022. 2
- [7] Yen-Chi Chen. A tutorial on kernel density estimation and recent advances. *Biostatistics & Epidemiology*, 1(1):161–187, 2017. 6
- [8] Krzysztof Choromanski, Valerii Likhoshesterov, David Dohan, Xingyou Song, Andreea Gane, Tamas Sarlos, Peter Hawkins, Jared Davis, David Belanger, Lucy Colwell, et al. Masked language modeling for proteins via linearly scalable long-context transformers. *arXiv preprint arXiv:2006.03555*, 2020. 5
- [9] Yufei Cui, Ziquan Liu, Xiangyu Liu, Xue Liu, Cong Wang, Tei-Wei Kuo, Chun Jason Xue, and Antoni B Chan. Bayesmil: A new probabilistic perspective on attention-based multiple instance learning for whole slide images. In *11th International Conference on Learning Representations (ICLR 2023)*, 2023. 1, 2, 4, 6, 7
- [10] Tri Dao, Dan Fu, Stefano Ermon, Atri Rudra, and Christopher Ré. Flashattention: Fast and memory-efficient exact attention with io-awareness. *Advances in Neural Information Processing Systems*, 35:16344–16359, 2022. 3, 5
- [11] Albert De La Chapelle and Heather Hampel. Clinical relevance of microsatellite instability in colorectal cancer. *Journal of Clinical Oncology*, 28(20):3380–3387, 2010. 6
- [12] Alexey Dosovitskiy, Lucas Beyer, Alexander Kolesnikov, Dirk Weissenborn, Xiaohua Zhai, Thomas Unterthiner, Mostafa Dehghani, Matthias Minderer, Georg Heigold, Sylvain Gelly, et al. An image is worth 16x16 words: Transformers for image recognition at scale. *arXiv preprint arXiv:2010.11929*, 2020. 4
- [13] Olga Fourkioti, Matt De Vries, and Chris Bakal. Camil: Context-aware multiple instance learning for cancer detection and subtyping in whole slide images. *arXiv preprint arXiv:2305.05314*, 2023. 1, 2, 3, 4, 5, 6
- [14] Dongchen Han, Xuran Pan, Yizeng Han, Shiji Song, and Gao Huang. Flatten transformer: Vision transformer using focused linear attention. In *Proceedings of the IEEE/CVF international conference on computer vision*, pages 5961–5971, 2023. 3, 5
- [15] Matthew G Hanna, Anil Parwani, and Sahussapont Joseph Sirintrapun. Whole slide imaging: technology and applications. *Advances in Anatomic Pathology*, 27(4):251–259, 2020. 1
- [16] Robert L Harrison. Introduction to monte carlo simulation. In *AIP conference proceedings*, page 17, 2010. 6
- [17] Chao-Hui Huang. Qust: Qupath extension for integrative whole slide image and spatial transcriptomics analysis. *arXiv preprint arXiv:2406.01613*, 2024. 2, 3
- [18] Maximilian Ilse, Jakub Tomczak, and Max Welling. Attention-based deep multiple instance learning. In *International conference on machine learning*, pages 2127–2136. PMLR, 2018. 1, 2, 6
- [19] Mingu Kang, Heon Song, Seonwook Park, Donggeun Yoo, and Sérgio Pereira. Benchmarking self-supervised learning on diverse pathology datasets. In *Proceedings of the IEEE/CVF Conference on Computer Vision and Pattern Recognition*, pages 3344–3354, 2023. 7
- [20] Angelos Katharopoulos, Apoorv Vyas, Nikolaos Pappas, and François Fleuret. Transformers are rnns: Fast autoregressive transformers with linear attention. In *International conference on machine learning*, pages 5156–5165. PMLR, 2020. 5
- [21] Jakob Nikolas Kather, Niels Halama, and Alexander Marx. 100,000 histological images of human colorectal cancer and healthy tissue. *Zenodo*, 5281:6, 2018. 8
- [22] Neeta Kumar, Ruchika Gupta, and Sanjay Gupta. Whole slide imaging (wsi) in pathology: current perspectives and future directions. *Journal of digital imaging*, 33(4):1034–1040, 2020. 1
- [23] Alona Levy-Jurgenson, Xavier Tekpli, Vessela N Kristensen, and Zohar Yakhini. Spatial transcriptomics inferred from pathology whole-slide images links tumor heterogeneity to survival in breast and lung cancer. *Scientific reports*, 10(1):18802, 2020. 2, 3
- [24] Bin Li, Yin Li, and Kevin W Eliceiri. Dual-stream multiple instance learning network for whole slide image classification with self-supervised contrastive learning. In *Proceedings of the IEEE/CVF conference on computer vision and pattern recognition*, pages 14318–14328, 2021. 2
- [25] Honglin Li, Yunlong Zhang, Pingyi Chen, Zhongyi Shui, Chenglu Zhu, and Lin Yang. Rethinking transformer for long

- contextual histopathology whole slide image analysis. *arXiv preprint arXiv:2410.14195*, 2024. 1, 2, 3, 4, 5
- [26] Tiancheng Lin, Zhimiao Yu, Hongyu Hu, Yi Xu, and Chang-Wen Chen. Interventional bag multi-instance learning on whole-slide pathological images. In *Proceedings of the IEEE/CVF Conference on Computer Vision and Pattern Recognition*, pages 19830–19839, 2023. 6
- [27] Ming Y Lu, Drew FK Williamson, Tiffany Y Chen, Richard J Chen, Matteo Barbieri, and Faisal Mahmood. Data-efficient and weakly supervised computational pathology on whole-slide images. *Nature biomedical engineering*, 5(6):555–570, 2021. 2, 6
- [28] Laura H Mariani, Sebastian Martini, Laura Barisoni, Pietro A Canetta, Jonathan P Troost, Jeffrey B Hodgins, Matthew Palmer, Avi Z Rosenberg, Kevin V Lemley, Hui-Ping Chien, et al. Interstitial fibrosis scored on whole-slide digital imaging of kidney biopsies is a predictor of outcome in proteinuric glomerulopathies. *Nephrology Dialysis Transplantation*, 33(2):310–318, 2018. 1
- [29] Paul Michel, Omer Levy, and Graham Neubig. Are sixteen heads really better than one? *Advances in neural information processing systems*, 32, 2019. 2, 6
- [30] Tan Nguyen, Tam Nguyen, Hai Do, Khai Nguyen, Vishwanath Saragadam, Minh Pham, Khuong Duy Nguyen, Nhat Ho, and Stanley Osher. Improving transformer with an admixture of attention heads. *Advances in neural information processing systems*, 35:27937–27952, 2022. 3
- [31] Tam Minh Nguyen, Tan Minh Nguyen, Dung DD Le, Duy Khuong Nguyen, Viet-Anh Tran, Richard Baraniuk, Nhat Ho, and Stanley Osher. Improving transformers with probabilistic attention keys. In *International Conference on Machine Learning*, pages 16595–16621. PMLR, 2022. 3, 4
- [32] Tan M Nguyen, Tam Nguyen, Long Bui, Hai Do, Duy Khuong Nguyen, Dung D Le, Hung Tran-The, Nhat Ho, Stan J Osher, and Richard G Baraniuk. A probabilistic framework for pruning transformers via a finite admixture of keys. In *ICASSP 2023-2023 IEEE International Conference on Acoustics, Speech and Signal Processing (ICASSP)*, pages 1–5. IEEE, 2023. 5
- [33] Kenta Oono and Taiji Suzuki. Graph neural networks exponentially lose expressive power for node classification. *arXiv preprint arXiv:1905.10947*, 2019. 2
- [34] Sharon Peled, Yosef E Maruvka, and Moti Freiman. Multi-cohort framework with cohort-aware attention and adversarial mutual-information minimization for whole slide image classification. *arXiv preprint arXiv:2409.11119*, 2024. 6
- [35] Pekka Ruusuvaari, Masi Valkonen, Kimmo Kartasalo, Mira Valkonen, Tapio Visakorpi, Matti Nykter, and Leena Latonen. Spatial analysis of histology in 3d: quantification and visualization of organ and tumor level tissue environment. *Heliyon*, 8(1), 2022. 2, 3
- [36] Zhuchen Shao, Hao Bian, Yang Chen, Yifeng Wang, Jian Zhang, Xiangyang Ji, et al. Transmil: Transformer based correlated multiple instance learning for whole slide image classification. *Advances in neural information processing systems*, 34:2136–2147, 2021. 2, 3, 5, 6, 7
- [37] Markus Svensén and Christopher M Bishop. Robust bayesian mixture modelling. *Neurocomputing*, 64:235–252, 2005. 5
- [38] Ashish Vaswani, Noam Shazeer, Niki Parmar, Jakob Uszkoreit, Llion Jones, Aidan N Gomez, Łukasz Kaiser, and Illia Polosukhin. Attention is all you need. *Advances in neural information processing systems*, 30, 2017. 6
- [39] Raghvendra Vishwakarma and Kirk J McManus. Chromosome instability; implications in cancer development, progression, and clinical outcomes. *Cancers*, 12(4):824, 2020. 6
- [40] Sinong Wang, Belinda Z Li, Madian Khabsa, Han Fang, and Hao Ma. Linformer: Self-attention with linear complexity. *arXiv preprint arXiv:2006.04768*, 2020. 5
- [41] Yunyang Xiong, Zhanpeng Zeng, Rudrasis Chakraborty, Mingxing Tan, Glenn Fung, Yin Li, and Vikas Singh. Nystromformer: A nystrom-based algorithm for approximating self-attention. In *Proceedings of the AAAI Conference on Artificial Intelligence*, pages 14138–14148, 2021. 3, 5
- [42] Hongrun Zhang, Yanda Meng, Yitian Zhao, Yihong Qiao, Xiaoyun Yang, Sarah E Coupland, and Yalin Zheng. Dtf-dmil: Double-tier feature distillation multiple instance learning for histopathology whole slide image classification. In *Proceedings of the IEEE/CVF Conference on Computer Vision and Pattern Recognition*, pages 18802–18812, 2022. 1, 2, 6
- [43] Tianfu Zhang, Heyan Huang, Chong Feng, and Longbing Cao. Enlivening redundant heads in multi-head self-attention for machine translation. In *EMNLP 2021-2021 Conference on Empirical Methods in Natural Language Processing, Proceedings*, 2021. 2, 6
- [44] Lan Zhao, Victor HF Lee, Michael K Ng, Hong Yan, and Maarten F Bijlsma. Molecular subtyping of cancer: current status and moving toward clinical applications. *Briefings in bioinformatics*, 20(2):572–584, 2019. 6
- [45] Yu Zhao, Zhenyu Lin, Kai Sun, Yidan Zhang, Junzhou Huang, Liansheng Wang, and Jianhua Yao. Setmil: spatial encoding transformer-based multiple instance learning for pathological image analysis. In *International Conference on Medical Image Computing and Computer-Assisted Intervention*, pages 66–76. Springer, 2022. 1, 2, 7
- [46] Yi Zheng, Rushin H Gindra, Emily J Green, Eric J Burks, Margrit Betke, Jennifer E Beane, and Vijaya B Kolachalama. A graph-transformer for whole slide image classification. *IEEE transactions on medical imaging*, 41(11):3003–3015, 2022. 2, 6, 7